Picturing China's Photovoltaic Energy Future: Insights from CMIP6 Climate Projections

Junhong Guo [a], Zhuo Chen [a], , Jing Meng [b], Heran Zheng [b], , Yuri Fan [c], Ling Ji [d], Xiuquan Wang [e*], Xi Liang [b*]

a: MOE Key Laboratory of Resource and Environmental, System Optimization, College of Environmental Science and Engineering, North China Electric Power University, Beijing 102206, China

b: Sustainable Finance and Infrastructure Transition, Bartlett School of Sustainable Construction, University College London, London, WC1E 6BT, United Kingdom

c: Department of Civil and Environmental Engineering, Brunel University, London, Uxbridge, Middlesex UB8 3PH, United Kingdom

d: School of Economics and Management, Beijing University of Technology, Beijing, 100124, China

e: School of Climate Change and Adaptation, University of Prince Edward Island, Charlottetown, Prince Edward Island, Canada C1A 4P3

*: *Corresponding author address: Xiuquan Wang (xiuquan.wang@gmail.com), Xi Liang (E-mail: xi.liang@ucl.ac.uk)*

Abstract

Vigorous development of solar photovoltaic energy (PV) is one of the key components to achieve China's "30•60 Dual-Carbon Target". In this study, by utilizing the outputs generated by CMIP6 models under different shared socioeconomic pathways (SSPs) and a physical PV model (GSEE), future changes in PV power generation across China are provided for the outlined carbon neutralization period (2051 to 2070). The results reveal distinct spatiotemporal characteristics in the changes in PV output across China. Overall, compared to the historical period, annual PV power generation is projected to decrease in northern regions and Tibet Plateau with a maximum decrease of ~ 4% under the high emission scenario (SSP585), while southern and central regions exhibit significant increases. Remarkably, under the green development pathway (SSP126), PV power generation is expected to rise by over 10% in these regions. The magnitude of decrease in the north and increase in the south is projected to become more pronounced with the continuous increase of future carbon emissions. It is anticipated that the three northern regions of China will experience greater decreases in PV power generation in winter compared to other seasons, especially under SSP585. Additionally, the southeast region shows the smallest increase in summer PV generation out of all seasons. Moreover, under SSP126 trajectory, most regions in China exhibit reduced inter-annual and intra-annual variability in PV generation compared to the historical levels. This suggests that pursuing a sustainable path could substantially mitigate potential risks associated with PV generation fluctuations in China.

Keywords: PV output, China, SSPs, projection, GSEE

Research highlights:

- A weighted CMIP6 ensemble was used to estimate the PV generation changes over China
- The northern and Tibet regions are projected to decrease in annual PV generation
- Annual PV output will increase in southern and central regions
- China's PV generation shows smaller inter- and intra-annual variability under SSP126

Word count: 6746 words.

Abbreviations:

CMIP5/6: Coupled Model Intercomparison Project, Phase 5/6
CN05: China grid daily dataset
CRMSE: centralized root mean squared error
ECMWF: European Center for Medium-Range Weather Forecasts
ERA5: the fifth generation ECMWF atmospheric reanalysis
GCM: Global climate model
GSEE: Global Solar Energy Estimator
IVS: Inter-annual variability skill score
MME: multi-model ensemble mean
NEA: China's National Energy Administration
PCC: Pearson correlation coefficient
PV: photovoltaic
RSDS: surface downwelling shortwave radiation
RSTD: ratio of standard deviations
SSPs: Shared Socioeconomic Pathways
TAS: near-surface air ambient temperature
TS: Taylor skill score

1. Introduction

The Paris Agreement in 2015 set a global warming target of limiting global warming to well below 2°C, preferably to 1.5°C, relative to pre-industrial levels [1]. Theoretically, to limit global warming to 1.5 °C at a 50% likelihood, global cumulative anthropogenic CO2 emissions should remain within a global carbon budget of around 580 Gt relative to 2010 level [2]. Achieving this ambitious target requires all participating countries to substantially enhance their emissions reduction willingness and efforts, peak their emissions as soon as feasible, and realize net-zero CO2 emissions by the mid-21st century [2, 3]. As the largest developing country and one of the top carbon emitters, China's pledge in 2020 to peak emissions before 2030 and achieve carbon neutrality before 2060 (the "30•60 Dual-Carbon Target"), demonstrates its willingness to take greater action on climate change and contribute to the Paris Agreement goals [4].

Renewable energy is a cornerstone in the reduction of CO2 emissions and consequent mitigation of changes in the global climatic system [5, 6]. Among various renewable energy sources, solar power generation plays a vital role in climate change mitigation options. Recent advances in solar technologies have made it the most cost-effective option for new electricity generation worldwide, which is expected to propel investment in the coming decades [7]. As the third largest renewable electricity technology after hydropower and wind, photovoltaic (PV) power saw remarkable growth in 2021, with a record increase of 179 TWh, making a 22% growth compared to the previous year [7].

China has emerged as a leading player in the global solar PV market. According to China's National Energy Administration (NEA), the country added 54.88 GW of solar PV capacity in 2021 comprising approximately 29.28 GW of distributed generation and 25.60 GW of centralized solar PV. Overall, China's market increased 21.5% in 2021 to reach 305.99 GW of cumulative capacity, with 35% from distributed generation and 65% from centralized plants [8]. In line with China's 14th Five-Year Plan for renewable energy released in 2022, the country shares its vision that an ambitious target of 33%

of electricity generation will come from renewables by 2025, including an 18% target for wind and solar technologies [7]. Therefore, a good knowledge of solar energy resources not only at present but also in the future is essential, in other words, a comprehensive and accurate estimation of where and how much PV power generation potential in China is crucial, and it can provide the scientific basis for the country's planning, energy policy formulation, and PV industry development in the future [9]. Meanwhile, policymakers need to consider the potential impact of climate change and possible development pathway options on PV output. Particularly in the current age, China is facing greater internal and external challenges than before, energy structure transformation, external geopolitical conflicts - understanding these factors is crucial for China's informed decision-making and sustainable development.

Apart from governmental policies, solar energy output is highly sensitive to climate change, due to hypothetical changes in the future atmospheric flow patterns, and even minor alterations in atmospheric conditions can have a significant impact on the power output [5, 10]. The relevant climate conditions for the productivity of solar power plants, such as solar radiation, ambient temperature, wind, snow and even the deposition of dust on the PV panels, are also subject to fluctuations resulting from changes in the frequency of weather and climate extremes under the context of climate change [11]. Of these factors, solar radiation availability, influenced by the scattering and absorption via clouds and aerosol concentration, is the most direct determinant of PV output [12]. Thus, reliable simulation data for solar radiation is the foundation for further PV power generation. However, obtaining observed irradiation data is often challenging due to high costs, maintenance and calibration requirements, and limited monitoring stations, especially in developing countries. These are not as readily available for observed irradiation stations as other common meteorological stations, i.e., temperature and precipitation [13-15]. Instead, empirical [14, 16, 17], physical [18, 19] and artificial intelligence models [13] are commonly employed to simulate and forecast the solar radiation amount and characteristics. Enormous studies indicated that artificial intelligence models, i.e., artificial neural networks, are promising for solar radiation

prediction [20-22].

To assess future changes in solar irradiance and relevant meteorological quantities for PV power production, comprehensive numerical models of the climate system are utilized [11]. Global climate models (GCM) have become the primary tools to investigate climate change, especially after the Coupled Model Intercomparison Project (CMIP) came into operation [23]. They can provide valuable insights into historical PV resource availability and projected future changes under various scenarios [10]. For instance, Wild, Folini [11] used a CMIP5 dataset to analyze the potential changes in surface temperature and solar radiation worldwide. They examined how these climate factors may affect solar power output from PV systems. However, they only utilized a fairly simplistic transformation method of solar power production, which considered on characteristics of the cell material, insolation and ambient air temperature. Zou, Wang [24] investigated the spatial distribution and long-term variation in historical surface solar radiation and future PV power output based on the CMIP5 models. They found that global dimming and brightening were observed before and after the 1990s and anthropogenic aerosols and cloudiness could be the main causes. The global potential photovoltaic power outputs were estimated in future scenarios using an empirical model that considered the photovoltaic cell's electrical efficiency and global solar radiation. Dutta, Chanda [12] explored the impact of climate change on global solar energy potential based on the monthly surface downwelling shortwave, temperature and wind speed from 5 CMIP6 GCM models. The results revealed substantial spatial variations in the projected PV changes across the world. For the computation of PV potential or concentrated solar power, the physical transformation process from climate factors to power output is simplified with empirical formulas. In China, Ji, Wu [25] used a GIS-based multiple-criteria decision-making approach, associated with the temperature and solar radiation from a regional climate model, to evaluate the potential PV capacity and generation in the future. Zhao, Huang [26] investigated the future PV-energy potential over China by downscaling output from 3 CMIP5 GCMs using the stepwise clustering analysis method. They concluded that

the PV changes in China were primarily contributed to the total radiation and sunshine duration.

To sum up, previous studies have utilized GCMs to analyze PV-related climatic simulations and projections globally, with a focus on radiation. However, few comprehensive studies on the PV power output in China have been conducted. In addition, a limited number of studies have incorporated the state-of-the-art CMIP6 models with updated Shared Socioeconomic Pathways (SSPs) scenarios for PV projections. Methodologically, empirical formulas and statistical methods (i.e., AI algorithm) are commonly employed to simulate PV output. Nonetheless, these methods irrespective of physical mechanism merely can be used to make a rough estimation for the impact of the projected changes in meteorological factors on solar power production. Moreover, they assume that the irradiance data in models is used for the horizontal plane, disregarding potential changes in irradiance when PV modules are mounted on tilted panels. Here, a model (GSEE) that incorporates physical mechanisms is employed to investigate the forthcoming variations in PV power generation in China. The GSEE is tailored to deliver a highly accurate simulation of real-world PV power generation, incorporating an array of physical mechanisms, encompassing meteorological conditions, PV panel specifications, and the intricate processes of physical transformation. The objective of this study is to assess and quantify the implications of the latest CMIP6 future climate projections on PV power generation in China, and address how PV power generation will evolve in China's carbon neutralization period under different socioeconomic pathways. The ultimate goal is to provide valuable insights to support the planning of China's renewable energy development and the formulation of carbon-neutral policies.

The research framework consists of three primary components, as depicted in Figure 1. First, key meteorological factors, namely downwelling shortwave radiation (RSDS) and near-surface air temperature (TAS) at a height of 2 meters, are validated historically using various spatiotemporal evaluation methods. In this step, the

performance of 14 CMIP6 Global Climate Models (GCMs) is assessed by comparing their outputs with observation data. The weight of each individual model is calculated based on model performance. The second step involves configuring and conducting experiments using a PV power generation model, known as GSEE. This model is used to simulate and analyze the characteristics of PV power generation under different climate emission scenarios. Finally, based on the driving data obtained from the previous steps and utilizing the GSEE PV model, future projections of changes in PV power generation across China are generated. These projections are examined and analyzed at multiple spatiotemporal scales. Ultimately, study findings are synthesized to offer a comprehensive discussion and decision support for national carbon neutrality policymaking.

==========

Place Figure 1 here

==========

2. Data and methods

2.1 CMIP6 outputs and observations

The RSDS and TAS from 14 different CMIP6 GCM outputs are used in this study (see Table S1 in the supplementary materials). The CMIP6 climate models are driven by a new set of emissions scenarios based on different socioeconomic assumptions, called Shared Socio-economic Pathways (SSPs). Three development scenarios are considered for China, corresponding to the SSPs: SSP1-2.6 (SSP126) is a sustainability scenario with a low forcing level of 2.6 W/m^2 by 2100, in other words, under this scenario, China will take a green development road and has the lowest challenges to mitigation and adaptation on climate change. SSP2-4.5 (SSP245) represents a central pathway in which the trends of development in China continue its historical patterns with a moderate anthropogenic radiative forcing level of 4.5 W/m^2 by 2100. The third pathway is the SSP5-8.5 (SSP585), which represents a fossil-fueled development scenario and the highest radiative forcing level in the future, suggesting that China will take a pathway with energy-intensive and fossil-based economies with

higher challenges to mitigation for climate change [12, 27]. In short, SSP126, SSP245 and SSP585 are used in this work to represent the “best”, “moderate” and “worst” scenarios of development in China.

To assess the reliability of the CMIP6 datasets, the gridded daily temperature with 0.25° spatial resolution over China is extracted from the CN05.1 dataset (hereinafter referred to as CN05). It was developed by the China Meteorological Administration (CMA) and is constructed based on the “anomaly approach” interpolation, with observations from 2,416 meteorological stations through quality control procedures and homogenization [23, 28]. In addition, developed by the European Center for Medium-Range Weather Forecasts (ECMWF), the ERA5 dataset provides a gridded surface downwelling solar radiation of 0.25° spatial resolution as the reference data to validate the simulated radiation abilities of the CMIP6 GCMs in China. As the different model outputs are available at different spatial resolutions, all GCM models are regridded to a common resolution of 0.25° using a bilinear interpolation method.

China is divided into 6 subregions on the basis of different climatic characteristics (Figure S1 and Table S2). The time span of 1995-2014 serves as the historical or baseline period for CMIP6 model validation against observations. The changes in PV generation output will be projected from 2051 to 2070. This 20-year period is defined as the carbon neutralization period and is determined with an extension from 9 years prior to and 10 years after the timing of China’s carbon neutralization target (2060).

2.2 PV power generation model

To simulate the PV electricity output in China, a numerical simulation model based on a physical mechanism is used, called the Global Solar Energy Estimator (GSEE) [29]. Required inputs are total horizontal solar irradiance (RSDS in CMIP6), the fraction of diffuse irradiance and ambient temperature (TAS in CMIP6). The fraction of diffuse irradiance can be calculated with the Boland–Ridley–Lauret model (BRL) module in

GSEE [30]. The temporal resolution of input data is flexible for GSEE. Various climate data with annual, seasonal, monthly, daily and hourly temporal resolution are supported in the model package. Besides, several panel-specific parameters, such as tilt and azimuth angles, installed panel capacity, panel tracking mode, system losses, etc., are input variables to calculate the PV power output [31]. The calculation procedure of this model is as follows:

First, irradiance on the plane of the PV panel is calculated. When a fixed azimuth angle and tilt angle are specified, the plane incidence angle α is defined:

$$\alpha = \cos^{-1}(\sin(h)\times\cos(t)+\cos(h)\times\sin(t)+\cos(a_p - a_s)) \quad (1)$$

where h is the sun altitude, t is the panel tilt, a_p and a_s are the panel azimuth and sun azimuth angle, respectively. Here, the panel tilt is given as a latitude-dependent function instead of a static value:

$$t = 0.35396\times\mathrm{lat}+16.84775 \quad (2)$$

where lat is the latitude of the grid point.

The total irradiance ($I_{tot,p}$) of the panel, including the direct and diffuse plane irradiance ($I_{dir,p}$ and $I_{dif,p}$) can then be computed from the total horizontal irradiance ($I_{tot,h}$) by

$$I_{tot,p} = I_{dir,p} + I_{dif,p} \quad (3)$$

$$I_{dir,p} = \frac{I_{dir,h}\times\cos(\alpha)}{\cos(\frac{\pi}{2}-a_s)} \quad (4)$$

$$I_{dif,p} = I_{dif,h}\times\frac{1+\cos(t)}{2} + A\times(I_{dir,h}+I_{dif,h})\times\frac{1-\cos(t)}{2} \quad (5)$$

where A is the surface albedo (default value 0.3).

In addition to solar irradiance, temperature on the panel (T_p) also affects the PV power output, and T_p can be roughly estimated from the ambient temperature (T_a) and total irradiance on the panel in the following way:

$$T_p = T_a + c_T\times I_{tot,p} \quad (6)$$

Where c_T represents how much the PV module is heated by solar radiation. This coefficient depends on the chosen panel material. Here, the empirical value (0.035 °CW^{-1} m^{-2}) is set for the crystalline silicon (c-Si) of panel, since it is the most prevailing semiconducting material used for PV systems [19].

Then, the PV power output (P_{out}) is calculated from total irradiance and panel temperature:

$$P_{out} = P_s \times \frac{I_{tot,p}}{I_s} \times \eta(I', T') \tag{7}$$

Where P_s is the PV output at standard test conditions of I_s = 1000 W/m^2 and T_s = 25 °C. The instantaneous relative efficiency (η) is calculated by a non-linear fitting function, depending on the chosen panel technology, and the empirical values for crystalline silicon (c-Si) are suggested by Huld, Gottschalg [32]. I' and T' are normalized parameters of panel total irradiance and temperature, which are defined as follows: $I' = I_{tot,p} / I_s$ and $T' = T_p / T_s$.

2.3 Model Evaluation Metrics

(1) Taylor diagram

In this study, a Taylor diagram [33] is used to assess how well the patterns between simulations and references. The diagram provides a graphical representation of three evaluation metrics. The azimuth angle reflects the Pearson correlation coefficient (PCC) of the spatial patterns. The radial distance from the origin represents the ratio of standard deviations (RSTD) and the distance from the simulation results to the reference is the centralized root mean squared error (CRMSE). Generally, in a Taylor diagram, if the PCC and RSTD are close to 1 and the CRMSE is close to the reference, the corresponding GCMs are considered with good simulation abilities [27]. Moreover, to analyze comprehensively these evaluation metrics from Taylor diagram, the Taylor

skill score is employed:

$$\mathrm{TS} = \frac{4(1+PCC)^4}{(RSTD+1/RSTD)^2(1+PCC')^4} \quad (1)$$

where TS is the Taylor skill score, PCC is the pattern correlation between the models and the observation, $RSTD$ is the ratio of spatial standard deviation in the models against that of the observation. PCC' is the maximum correlation coefficient attainable (here is 0.999). The score equals 1 for a perfect match between the model and observation, and 0 for an inverse model performance [34].

(2) inter-annual variability skill score (IVS)

It is important to evaluate the performance of models in simulating temporal variation of observation. Here, the IVS score described by Jiang, Li [35] is used to quantify the similarity of inter-annual variability between modeled and observed variables, defined as follows:

$$IVS = \left(\frac{STD_{\mathrm{g}}}{STD_{\mathrm{o}}} - \frac{STD_o}{STD_g}\right)^2 \quad (2)$$

where STD_{g} and STD_o denote the inter-annual standard deviation of GCM simulations and observations, respectively. Smaller IVS values represent a better agreement on inter-annual variability between the simulations and observations.

(3) Weight calculation

Due to the uncertainty of a single GCM, a multi-model ensemble mean is often used to reduce the uncertainties in climate projections. However, using the simple equal-weighted averaging method could cause one problem, that is, the highly skillful models can be underestimated while relatively poor models are overestimated to some extent. Thus, a weighted method [36] instead of the traditional arithmetical average is defined as follows:

$$R_i = \frac{\sum_{i=1}^{N} S_i}{S_i} \quad (3)$$

$$W_i = \frac{\sum_{i=1}^{N} R_i}{R_i} \quad (4)$$

Where S_i denotes the ranking position (including Taylor and IVS scores) among all models for an individual model i; R_i can be considered the combined performance indicator of each model; W_i is the weight of each model; N is the number of models.

3. Results

3.1 Validation of CMIP6 models

The surface downwelling shortwave radiation (RSDS) and near-surface air temperature (TAS) are the most key meteorological factors for projecting PV output, as direct input parameters to the GSEE numerical simulation model. There are discrepancies between CMIP6 models in simulating the RSDS and TAS over China. Thus, their simulation abilities are evaluated in reproducing the spatiotemporal characteristics observed in the EAR5 and CN05 datasets. Then the rank and weight of individual models are calculated based on the comprehensive analysis of the impact degree for all models. This approach allows us to evaluate and compare the simulation abilities of CMIP6 models in simulating RSDS and TAS over China, providing valuable insights into their reliability and suitability for PV power output projections.

The differences in annual mean RSDS and TAS spatial fields between CMIP6 multi-model ensemble mean and observations (ERA5 and CN05) in the historical period are shown in Figure 2. In general, there is good agreement in spatial distribution between the simulation and observational data sets. For RSDS, the highest radiation occurs over western China, especially in the west of the Tibetan Plateau, while the lowest

radiation is observed over eastern China. In terms of TAS, the warm center is situated in the southeast of China, while the northeast and Tibet have lower temperature relative to other areas in China. However, there are some biases in local regions. The biases of RSDS in most regions of China are kept at 20 W/m^2 except for the overestimation in some southern provinces, such as Guizhou and Guangxi. Additionally, although the CMIP6 ensemble mean can reproduce the spatial distribution of annual mean temperature reasonably, particularly in eastern China with the bias of ~1°C, these models tend to underestimate the temperature magnitude in the west. Notably, there are very large negative biases in the western edge of the Tibetan Plateau and Xinjiang.

==========

Place Figure 2 here

==========

Figure 3 shows the quantified assessment results in the Taylor diagram. Overall, the performance in simulating the TAS from GCM models is better than the RSDS. The correlation coefficient in the spatial pattern of TAS exceeds 0.9 for all models and is above 0.95 (i.e., CanESM5, CESM2-WACCM, MRI-ESM2-0 and NorESM2-MM). Most models have a higher RSTD value, ranging from 0.5 to 0.75. In contrast to temperature, CMIP6 models derived from the RSDS show more scattered in the Taylor diagram, indicating there are more uncertainties in simulating the historical surface downwelling shortwave radiation. When compared with ERA5, the BCC-CSM2-MR and IPSL-CM6A-LR are found to be the least correlation among the 14 models. The remaining models in the CMIP6 family have a correlation ranging between 0.8 and 0.95.

==========

Place Figures 3-4 here

==========

To provide a concise summary of the simulation skill in each CMIP6 model with respect to the spatial pattern, these assessment indices (i.e., PCC, RSTD and CRSME) from the Taylor diagram are calculated as the Taylor skill score (Figure 4). As described, relative to the RSDS, the CMIP6 models tend to show superior spatial simulation skills

in simulating the TAS, as the score values are consistently more than 0.8 and even up to 0.9. Actually, most CMIP6 models also perform well in simulating the spatial distribution of the RSDS over China, except for BCC-CSM2-MR and IPSL-CM6A-LR. The best model is CMCC-ESM2 with the highest score of exceeding 0.9 in simulating the RSDS against the ERA5 dataset.

==========

Place Figure 5 here

==========

Besides the mean climate state in the spatial distribution, the differences in interannual variability between CMIP6 simulations and the reference data are further estimated using the IVS method and the results are shown in Figure 5. The IVS values indicate the similarity of inter-annual variability between the CMIP6 models and the observation, with smaller values indicating better performance for the model. For RSDS, except for CanESM5, CESM2-WACCM and ACCESS-ESM1-5, most models have lower IVS values. In comparison, the overall IVS values in simulating the TAS are smaller than those for RSDS. CanESM5 has the highest IVS in simulating for TAS with 1.326 and 0.566 for RSDS, implying it can not well capture the inter-annual variability as well as the observation. The results also show the ability of each model to simulate the inter-annual variability is not totally equal between RSDS and TAS. For example, CNRM-CM6-1 and IPSL-CM6A-LR demonstrate relatively large IVS values in simulating the TAS while the values are smaller in the RSDS. It is noteworthy that the model's performance seems to be independent between the Taylor skill scores and IVS, as some models with relatively poor mean-state simulation in spatial patterns (i.e., BCC-CSM2-MR) can exhibit better skill in simulating the inter-annual variability.

Figure S2 shows the weights of CMIP6 models based on the evaluation of the spatial distribution and inter-annual variability. The results show that the CMCC-ESM2, CESM2-WACCM, INM-CM5-0 and MRI-ESM2-0 have larger weights than other models, while the weights of IPSL-CM6A-LR and MIROC6 are smaller due to their poor performance.

3.2 Projections of changes in PV power generation

3.2.1 Annual changes

Future annual PV power generation changes and the trend in spatial distributions under different socioeconomic pathways over China are analyzed in this section. Figure 6 illustrates the projected weighted MME PV differences in the carbon neutralization period (2051-2070) relative to the baseline period (1995-2014). Overall, the geographical distributions between the absolute and relative PV changes in China are similar. Changes in PV power generation show distinct characteristics in different regions. While the magnitudes may differ, there is a distinct division for the change sign from the northwest to the southeast of China, which interestingly aligns closely with the famous “Hu Huanyong line”. Specifically, the general tendency is a cutback in the north and west, which are more pronounced if no greenhouse gas mitigation strategies are employed (i.e., a decrease of ~4% under SSP585). Conversely, an increase in PV power generation is evident in the southeastern parts of China with some regions, such as Hunan and Chongqing, experiencing an approximate 10% increase under the SSP126 scenario. In view of emission scenarios, a transition from SSP126 to SSP585 leads to a smaller increase in PV generation in the southeast, while a larger decrease is found in the north and west of China.

==========

Place Figures 6-7 here

==========

A decreasing trend is detected in most regions of the north (Figure 7), and the annual mean PV power will decrease by above 1000 Wh/year. The utmost decrease (about 3000 Wh) is expected in the west of Mongolia with a decreasing trend extending southwestward in the spatial pattern. It is noteworthy that the decreasing trend is statistically significant, especially for SSP585. Conversely, southern China will witness an increasing trend in PV power during this period, except for a slight decrease in the SSP126 scenario. Meanwhile, it is clear that these changes and tendencies are more

pronounced under scenarios of stronger radiative forcing, although SSP245 shows a more significant increase in the PV output.

The inter-annual variability in spatial distribution, which is quantified as the ratio of standard deviation to the mean annual PV power between years, is presented in Figure 7(d-f). Under SSP126 and SSP245 emission scenarios, the inter-annual variability is smaller in the neutralization period than that in the baseline, especially for the central regions, such as Hebei. In addition, as radiative forcing intensifies in the future, most regions over China show an increasing tendency in inter-annual variability. The highest interannual variability (more than 20%) is projected by the models in the west of China.

3.2.2 Changes in annual cycle

Figure 8 presents the percentage changes in seasonal photovoltaic generation under the different SSP scenarios and the regional mean changes in season over entire China are calculated in Table 1. The results show that the spatial distribution of changes in PV electricity generation in season is analogous with that in annual. Overall, the magnitude of decrease (increase) in the north (south) is projected to amplify (shrink) with the continuous increase of future emissions. Nonetheless, there are distinct differences in the spatial distributions and change magnitude among different seasons.

In general, the SSP126 scenario shows a larger increase in PV electricity generation compared to other scenarios, though a slight decrease (~2%) is found in the west and northwest of China. Particularly in winter and autumn, the regional mean PV electricity generation in China is projected to rise by 3.55% and 3.18% respectively, relative to the historical period. In detail, the maximum increase of up to 16% will be seen in the east of Sichuan and Chongqing in winter and autumn. Under SSP245, except for spring, the entire PV is likely to have a marginal increase (below 1%) during the other seasons. However, certain regions, such as the north of Xinjiang, Tibet, are expected to decrease prominently in PV generation, with the spatial patterns and magnitude of

decrease extending with emissions increase. During the carbon neutralization period, the overall regional mean PV power generation in summer and autumn over China seems to have no major changes compared with the historical period under the intensive GHG emissions (SSP585), whereas the PV production will decrease slightly (0.81%) in winter and spring. It is expedient to note that when calculating the change in PV power production across China as a whole, the change sign or magnitude in different regions may more or less cancel each other out. Therefore, it is necessary to evaluate the changes in PV power production across each subregion of China individually.

==========

Place Figure 8 here

==========

Figure 9 exhibits the seasonal percentage changes in PV electricity generation for six subregions in China. The results show that three northern regions (i.e., NE, N and NW) are expected to have smaller PV power generation in most seasons relative to the historical period. The magnitude of the decrease is larger in winter than in other seasons and is particularly significant under SSP585. For the Tibet Plateau, the seasonal mean PV power generation tends to decrease in the future and the differences between seasons and SSP scenarios are marginal. Meanwhile, the PV power in Tibet is projected to have the most decrease among subregions, particularly under SSP245 and SSP585 scenarios. The reverse is the case for two southern regions. There is a slight increase in the range of 3% to 6% over the southwest region under the SSP126 emission scenario, with minimal differences between SSP245 and SSP585. Worthy of note is that the southeast region (SE) will experience the largest increasing magnitude relative to other subregions, especially in winter with an increase of above 12%. However, the corresponding magnitude in summer is smaller relative to other seasons.

==========

Place Figure 9 and Table 1 here

==========

To further investigate the intra-annual variability of PV production, monthly changes in the carbon neutralization period relative to the baseline for six subregions in China are shown in Figure 10. Additionally, the standard deviation to measure the intra-annual variability is calculated based on the historical and future monthly PV power results and then compares the difference between these periods (Table 2).

==========

Place Figure 10 here

==========

The differences in monthly PV power generation help to explain the seasonal changes to some extent. In the northeast and north regions, the pattern appears consistent, with nearly all months showing an increasing PV production in the carbon neutralization period under the SSP126 scenario, while there are notable differences among months under other scenarios. For example, during some warm months (i.e., from May to October), the projected PV power generation tends to increase by 3%~5% over the northwest. Compared with the baseline, the PV will decrease by 5% or even more in some cold months in winter and spring. For the northwest and west regions, it is evident that most months are projected to have a decreasing PV electricity generation relative to the baseline, especially for the west under the SSP585 scenario. However, the opposite trend is observed in the southwest and southeast regions. Compared with the historical period, the southeast shows a consistent increase in PV production for all the months, with the largest increase (above 10% in SSP126) in cold months and the smallest increase in June and July. In addition, the range of variation (indicated by the lengths of the boxes and whiskers) seems to be larger in cold months for all subregions, suggesting more uncertainties among CMIP6 models in the future projection of PV power generation in these months.

According to Table 2, except for the southwest and southeast regions, there are no major changes expected in the intra-annual variability of PV power generation during the neutralization period, since the differences in monthly standard deviation between the historical and future periods are relatively small. However, when considering

SSP126, the north region tends to decrease by 2.59% in PV power generation intra-annual variability. Conversely, for the northwest, the intra-annual variability is likely to increase by 2.39% and 2.69% under the SSP245 and SSP585 scenarios, respectively. For two southern regions, there is a clear tendency towards a significant decrease in the intra-annual variability. For example, compared with the baseline period, the intra-annual variability in the southeast will reduce by 12.35%. Overall, the intra-annual variability in the three northern regions and Tibet is projected to have an increasing tendency with the rise in emissions. Under the SSP126 scenario, all subregions show a lower intra-annual variability than that in the historical period.

==========

Place Table 2 here

==========

4. Discussions

Vigorous PV development is one of the key components to achieving China's "30-60" dual carbon targets. Evaluating the influence of various climate or socioeconomic scenarios on PV power generation is crucial. This study depicts a picture of future changes in PV power generation for the carbon neutralization period in China, utilizing the CMIP6 models under different shared socioeconomic pathways.

Overall, the irradiance is larger in the west than that in the east and north of China. Theoretically, the corresponding PV power generation should be more abundant in the western regions, such as Tibet and Xinjiang. However, in reality, the majority of giant PV farms are concentrated in the east. According to the statistics from China's National Energy Administration, the installed capacities in Shandong, Hebei, Jiangsu and Zhejiang are larger than other provinces in China and only Ningxia is in the top 10 list for installed capacity [37]. This discrepancy may seem unusual in that the regions with richer irradiance have no faster development. The reason is in various aspects. The technical, policy and economic factors may constrain the development of PV in these regions. It is recognized that the PV power output has stochastic, unstable and non-

durable characteristics and is affected predominantly by meteorological factors, such as solar radiation, ambient temperature, wind, snow, and so on [11]. Additionally, due to the high cost of power grid construction and relatively immature storage technology, the produced PV power relies heavily on local consumption. For the same regions with sparse populations and underdeveloped economies like Tibet, currently, it might not be enough suitable to build a giant centered PV plant and complex power grid when considering the cost and environmental protection. Instead, hybrid multiple renewable energies (i.e., wind, solar and geothermal) may be preferable for the locals [38, 39]. Nevertheless, in the foreseeable future, or more optimistically before China's carbon neutralization target deadline, with the construction of robustly large interconnected power networks and improvement of energy storage technologies, China will continue to promote the strategy of "West-East Power Transmission" to achieve the carbon neutralization goals[40].

Looking ahead, as far as spatial characteristics are concerned, the results show that annual and seasonal PV power generation will decrease in the north and Tibet regions relative to the historical period. In addition, with the increasing carbon emissions, the decreasing tendency of PV electricity generation is projected to extend southwestward from the west of Mongolia, implying that albeit modestly PV power generation will be inevitably influenced if carbon emission policies are not implemented. However, as mentioned by Abolude, Zhou [41], the decrease in future renewable energy potential does not imply a halt or reduction of renewable energy investment, nor does it pose a significant threat to commercialization and marketability. Instead, it should be seen as an early warning that a continuous increase in emissions is likely to impact PV power production in China, albeit these risks could be avoided and mitigated through technological improvements. On the contrary, the south and central regions are expected to have an apparent increase in PV power generation in the neutralization period. It is expedient to note that in recent two years some provinces with a larger installed capacity in China, such as Shandong, Hebei, Jiangsu and Zhejiang, have seen a greater proportion of distributed PV power generation. The result will

undoubtedly serve as a great encouragement to the PV industry in these regions of China.

Despite overall satisfactory performance in most regions of China, there are still notable biases observed in certain areas when compared to actual observations, particularly in some southern provinces and western edges of China. It is worth mentioning that these biases have the potential to influence future climate projections [42]. Consequently, it is prudent to exercise caution when interpreting future projections in these particular regions, even though the focus of the projections is on changes rather than absolute values.

In terms of temporal variability, under SSP126 and SSP245 emission scenarios, the inter-annual variability is smaller in the neutralization period versus the baseline. Nonetheless, with the enhancement of the radiative forcing in the future (SSP585), most regions over China demonstrate an increasing trend in inter-annual variability, particularly in the west of China, even more than 20% relative to the reference period. Generally, understanding the potential economic returns on an initial investment in PV systems is crucial for utilities and residential customers alike [43]. The inter-annual variability of power output between different years is a key factor for the economic feasibility of a renewable power station because whether the farm's expected energy yield will remain stable (with smaller inter-annual variability) during its lifetime can determine the success or failure of the power farm project [5]. In the neutralization period, the intra-annual variability of PV power generation in the southwest and southeast regions is smaller (exceeding -10%) than that in the historical period. This could benefit for PV plant owners in these regions because the higher intra-annual variability will directly lead to more variables in the injection of the produced energy into the electrical grid, potentially resulting in supply-demand balancing issues and decreased PV farm’s profitability in the electricity market [5]. Under SSP245 and SSP585 scenarios, the intra-annual variability in the northwest is likely to increase slightly, but for SSP126, all subregions in China show a smaller intra-annual variability

than that in the historical period. In summary, the results suggest that China's commitment to green development can reduce risks associated with inter-annual and intra-annual variabilities in PV power generation in the long run.

Some attributions can explain the temper-spatial changes in PV generation in China, as suggested by previous studies. One important factor is the presence of anthropogenic aerosols and other air pollutants, which have a significant impact on surface solar radiation and PV power [24]. The results show that in winter, PV power generation shows a decreasing trend in the north, especially under the SSP585 emission scenario. Li, Wagner [44] evaluated the impact of aerosols on PV generation and came to a similar conclusion. They found aerosol-related annual average reductions of point-of-array irradiance in northern and eastern China to be about 20%-25%. In winter, aerosols have comparable impacts on clouds. Improving air quality in China would increase the efficiency of solar PV generation. It may be a key explanation for the significant decrease in PV power generation in the north of China under the fossil-fueled development scenario (SSP585). Implementing strict air pollution control measures and reducing fossil fuel consumption will increase surface radiation, improving PV power generation [45]. Southeastern China is projected to have more PV power generation in the neutralization period, but the increasing magnitude is smaller in summer than that in other seasons. This is explained by the higher percentage of monsoon cloud cover in summer because cloud fraction influences solar radiation more than any other parameters [10]. The climate of the southeast in summer is characterized by wetter conditions from the East Asian monsoon, resulting in lower all-sky radiation caused by cloud scattering, reflection and absorption [11, 46].

Finally, it is crucial to acknowledge the presence of inherent uncertainties in projecting future climate change. These uncertainties arise from various factors, such as GCM driving data, model structure and parameters, and observational data, among others [47, 48]. In this study, the weighted ensemble mean method was employed to alleviate uncertainties stemming from the driving data. Additionally, it should be noted that

biases observed in certain regions of China could also be attributed to limitations in observational data, such as the sparse coverage of observation stations in the complex terrain of the Tibetan Plateau. To address these uncertainties, future research endeavors can consider employing bias correction techniques, incorporating a broader range of GCMs, and utilizing downscaling methods, to further reduce these uncertainties in future climate projections, enabling more accurate and reliable assessments of climate change impacts at regional and local scales.

5. Conclusion

When planning the roadmap of renewable energy development to achieve the carbon neutralization target, investigation of the long-term variation and spatial distribution of PV power output is of great importance and essential for China. In this study, the output from 14 weighted CMIP6 GCMs was used to estimate the PV power generation changes in China under 3 different socioeconomic pathways during the carbon neutralization period (2051-2070).

Overall, the CMIP6 models demonstrate a satisfactory capability in reproducing the spatial and temporal distribution of key meteorological factors affecting photovoltaic systems, such as downward shortwave radiation (RSDS) and near-surface air temperature (TAS). This conclusion is drawn from the evaluation using Taylor and IVS scores. However, biases persist in certain regions of China, potentially due to limitations in the available observational data, including sparse coverage of observation stations, particularly in complex terrain areas like the Tibetan Plateau. To reduce the uncertainties arising from inter-model variability, the rank and weight of individual models are calculated based on the comprehensive analysis of the impact degree for all models. By assigning appropriate ranks and weights to the models, this study aimed to enhance the reliability and robustness of the projections while reducing the influence of any single model’s biases.

The changes in PV power generation in China show distinct spatiotemporal characteristics. Overall, compared with the historical period, the annual PV power generation will decrease in the north and Tibet regions, with a maximum ~4% decline under SSP585. This suggests that, even if the decline is relatively modest, PV power generation will inevitably be influenced if carbon emission reduction policies are not implemented. This finding should serve as an initial warning that continued emission increases are likely to impact PV power production in China. While the southern and central regions are expected to have an apparent increase, i.e., there is the largest increase of above 10% in the PV power generation under SSP126 in the neutralization period. This anticipated expansion should provide substantial encouragement to the PV industry in these regions. The spatial distribution of seasonal changes in PV electricity generation is analogous to that in annual. Magnitudes of northern decrease and southern increase are projected to amplify with the continuous increase of future carbon emissions. Three northern regions of China are expected to have smaller PV power generation in winter than that in other seasons, especially under SSP585. In summer, the increasing magnitude of PV power generation in the southeast is the smallest among seasons. The changes in monthly PV power generation further explained the different features in season. Moreover, under SSP126, most regions over China show a smaller inter-annual and intra-annual variability than that in the historical period, suggesting that pursuing a green development pathway could greatly mitigate PV generation variability risks, as higher intra-annual variability often leads to greater fluctuations in energy injection into the electrical grid.

To sum up, these findings offer valuable insights into the potential changes in PV power generation across different regions of China during the country's carbon neutralization period. They highlight the importance of implementing effective emission reduction policies and provide guidance for policymakers and stakeholders in the PV industry.

Author Contributions

Junhong Guo conceptualized this research. Xiuquan Wang designed the research methods. Jing Meng and Heran Zheng processed and analyzed the data. Zhuo Chen, Ling Ji and Xi Liang made revisions to the paper. All the authors conceived the paper and designed the research.

Acknowledgments

This study is supported by the Natural Science Foundation of China (Grant No. 62073134).

Declaration of Interests

The authors declare no competing interests.

Table Captions

Table 1. The regional annual and seasonal mean changes in PV power generation over entire China (Unit:%). The first column represents the abbreviations of annual, winter, spring and summer, respectively.

Table 2. The changes of intra-annual variability in PV power generation under SSP scenarios relative to the baseline period over six subregions of China (Unit: %).

Table 1. The regional annual and seasonal mean changes in PV power generation over entire China (Unit:%). The first column represents annual, winter, spring and summer, respectively.

	SSP126	SSP245	SSP585
Annual	2.76	0.35	-0.34
Winter	3.53	0.30	-0.51
Spring	2.30	-0.04	-0.81
Summer	2.49	0.57	0.10
Autumn	3.18	0.77	0.13

Table 2. The changes of intra-annual variability in PV power generation under SSP scenarios relative to the baseline period over six subregions of China (Unit: %).

	Northeast	North	Northwest	Tibet Plateau	Southwest	Southeast
SSP126	-0.34	-2.59	-0.74	-1.72	-6.73	-12.35
SSP245	-0.03	-0.15	2.39	-0.46	-6.01	-8.22
SSP585	1.48	0.90	2.69	1.30	-8.90	-10.53

Figure Captions

Figure 1. Research framework.

Figure 2. The differences in annual RSDS and TAS spatial fields between CMIP6 multi-model mean simulation and observation. The first column (OBS) represents ERA5 for RSDS and CN05 for TAS observations. The second column (SIM) is the multi-model ensemble mean simulation. The third row (BIAS) shows the bias between simulation and observation.

Figure 3. Taylor diagram for simulations and reference values of the surface downwelling shortwave radiation (RSDS) and ambient temperature (TAS) in China for the historical period of 1995-2014. “1-12” denotes the simulation fields of the CMIP6 models and “REF” represents the reference fields of ERA5 for RSDS and CN05 for TAS.

Figure 4. Taylor skill score of each model of CMIP6 in simulating the spatial patterns of the mean state of the surface downwelling shortwave radiation (RSDS, left) and ambient temperature (TAS, right) over China during 1995-2014.

Figure 5. IVS score of each model of CMIP6 in simulating the spatial patterns of the mean state of the surface downwelling shortwave radiation (RSDS, left) and ambient temperature (TAS, right) over China during 1995-2014.

Figure 6. Future changes in annual PV generation relative to the historical period (2051-2070) under the SSP126 (first column), SSP245 (second column) and SSP585 (third column) scenarios. The first row (a-c) shows the absolute changes (unit: kWh) and the second (d-f) shows the relative changes (unit: %).

Figure 7. Spatial trends (a-c) and inter-annual variability d-f) of potential photovoltaic power for multi-model ensemble mean over China under the SSP126 (a, d), SSP245 (d, e) and SSP585 (c, f) scenarios during the period of 2051-2070 (light gray dot covered area indicates the statistically significant trends with a student-t statistical significance level of 5%).

Figure 8. Percentage changes in seasonal photovoltaic generation under the SSP126 (first column), SSP245 (second column) and SSP585 (third column) scenarios. Maps

show differences between 2051-2070 and 1995-2014 in the multi-model mean, calculated as future minus reference. The rows depict the changes in winter, spring, summer and autumn.

Figure 9. The spider map of changes in seasonal PV generation over the subregions of China under SSP126, SSP245 and SSP585 scenarios (Unit: %). The five axes of spider map represent the changes in annual, winter, spring, summer and autumn.

Figure 10. Box-whisker plots of PV power generation changes (%) for CMIP6 models in six subregions over China under SSP126, SSP245 and SSP585 scenarios. The whiskers indicate the minimum and maximum changes, and the boxes represent the 25th to 75th percentile. The black dotted line represents the baseline of the historical period and the solid lines are the mean line of different scenarios.

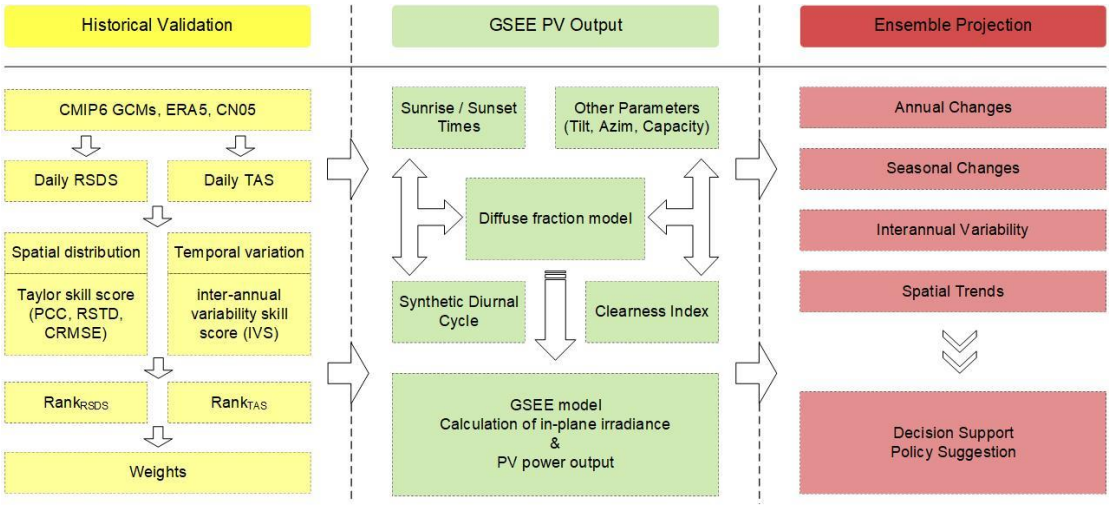

Figure 1. Research framework.

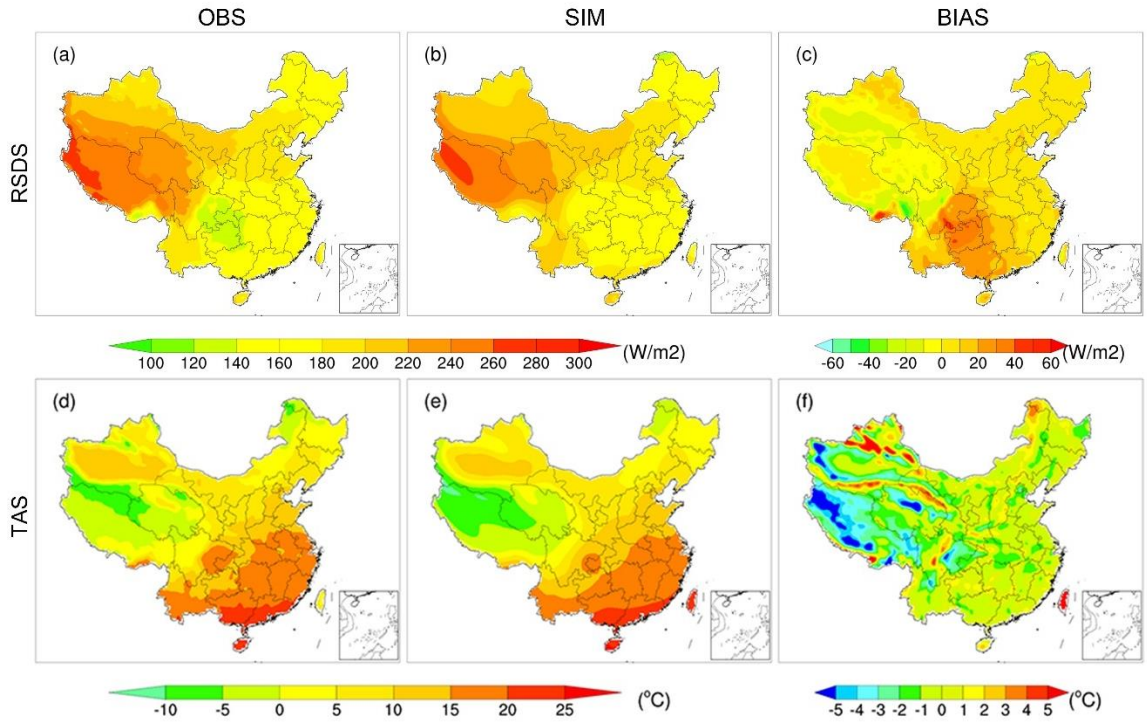

Figure 2. The differences in annual RSDS and TAS spatial fields between CMIP6 multi-model mean simulation and observation. The first column (OBS) represents ERA5 for RSDS and CN05 for TAS observations. The second column (SIM) is the multi-model ensemble mean simulation. The third row (BIAS) shows the bias between simulation and observation.

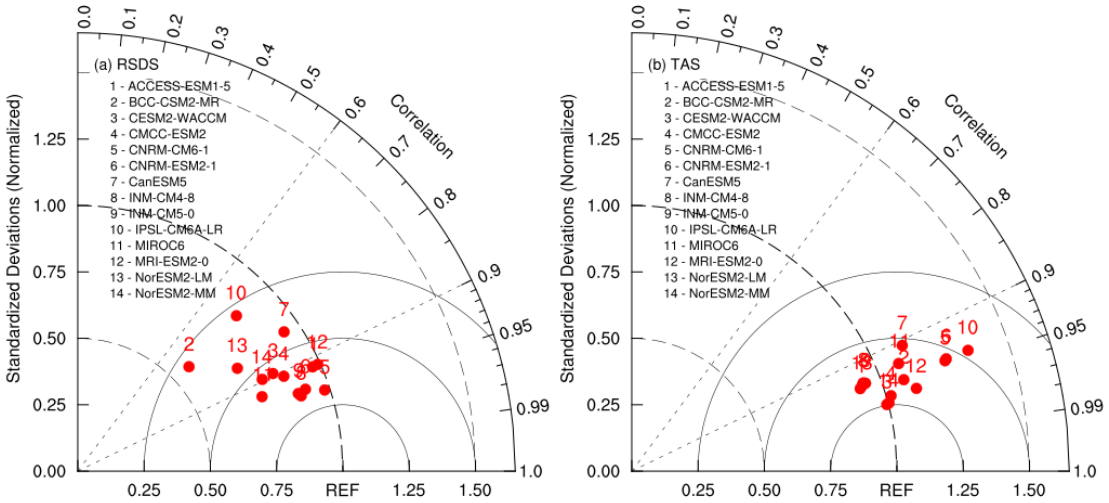

Figure 3. Taylor diagram for simulations and reference values of the surface downwelling shortwave radiation (RSDS) and ambient temperature (TAS) in China for the historical period of 1995-2014. “1-12” denotes the simulation fields of the CMIP6 models and “REF” represents the reference fields of ERA5 for RSDS and CN05 for TAS.

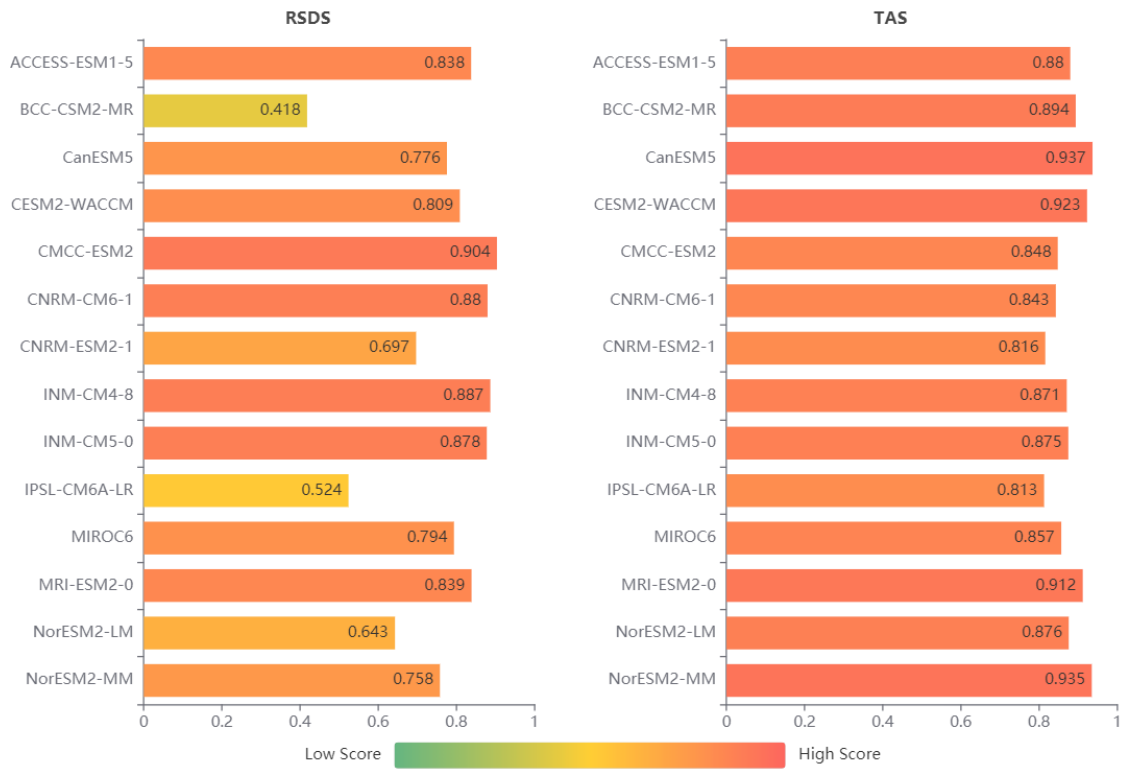

Figure 4. Taylor skill score of each model of CMIP6 in simulating the spatial patterns of the mean state of the surface downwelling shortwave radiation (RSDS, left) and ambient temperature (TAS, right) over China during 1995-2014.

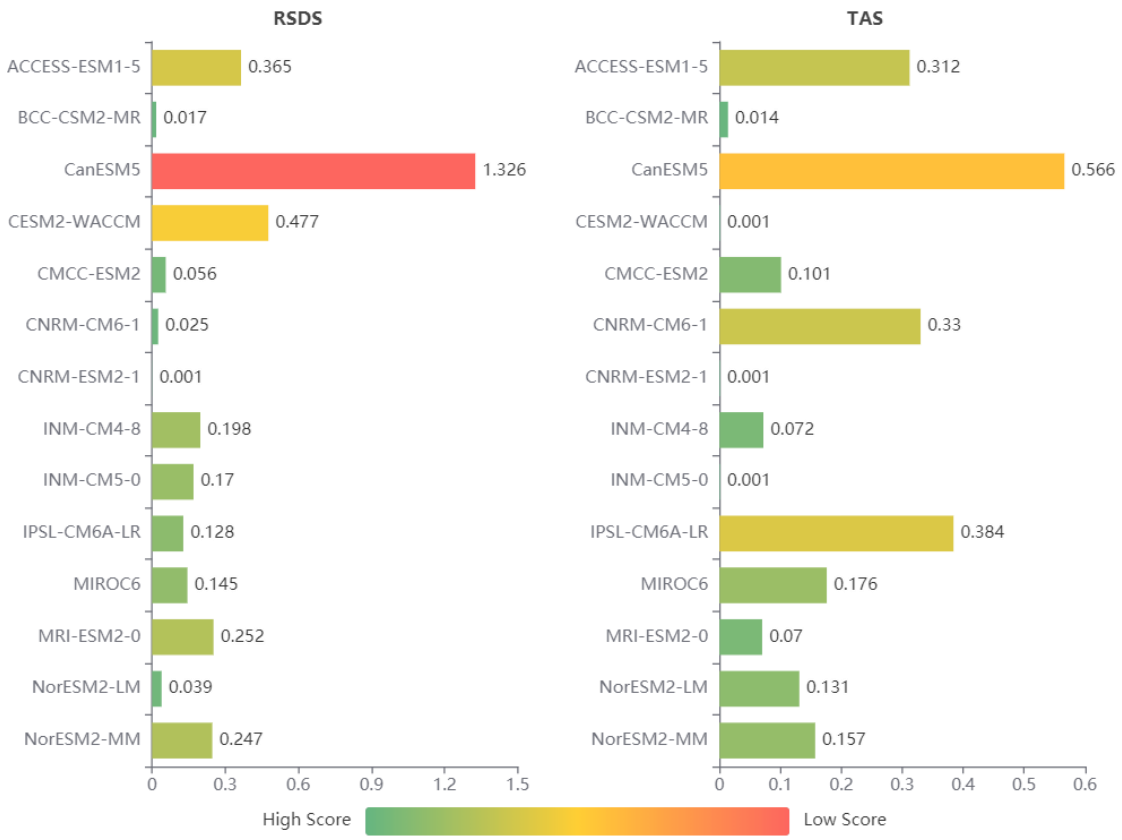

Figure 5. IVS score of each model of CMIP6 in simulating the spatial patterns of the mean state of the surface downwelling shortwave radiation (RSDS, left) and ambient temperature (TAS, right) over China during 1995-2014.

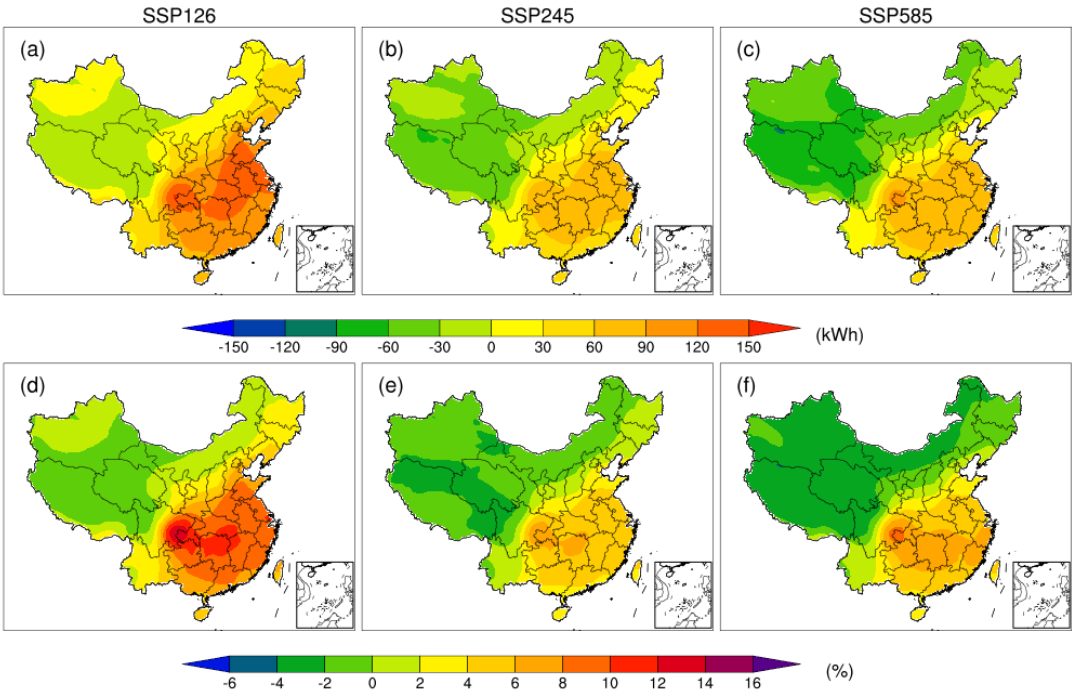

Figure 6. Future changes in annual PV generation relative to the historical period (2051-2070) under the SSP126 (first column), SSP245 (second column) and SSP585 (third column) scenarios. The first row (a-c) shows the absolute changes (unit: kWh) and the second (d-f) shows the relative changes (unit: %).

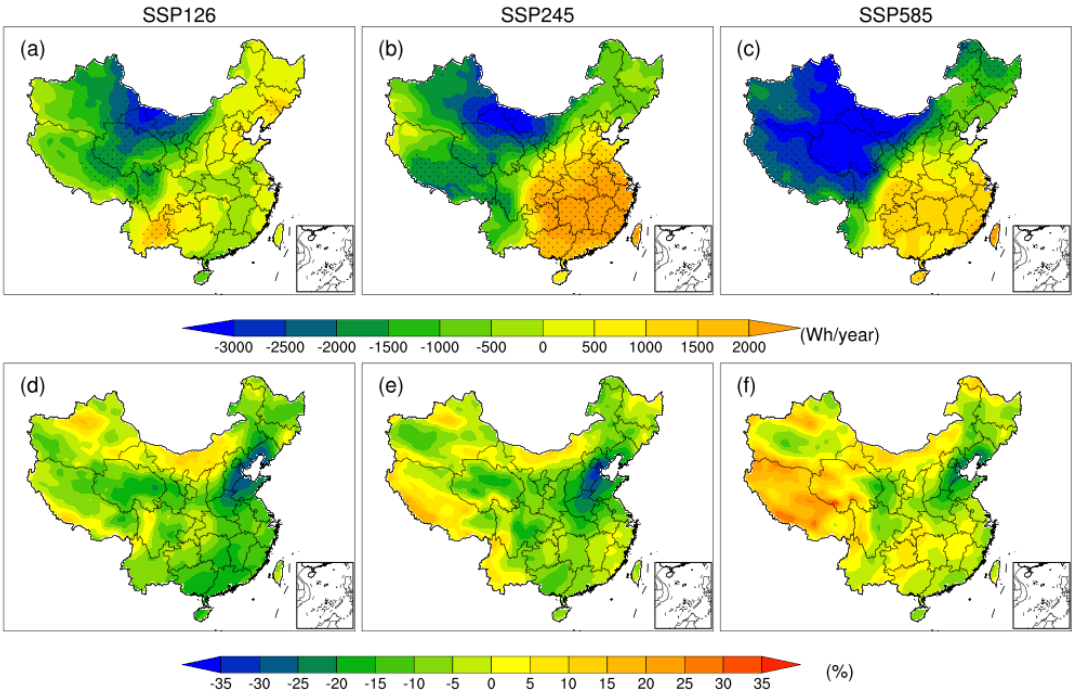

Figure 7. Spatial trends (a-c) and inter-annual variability d-f) of potential photovoltaic power for multi-model ensemble mean over China under the SSP126 (a, d), SSP245 (d, e) and SSP585 (c, f) scenarios during the period of 2051-2070 (light gray dot covered area indicates the statistically significant trends with a student-t statistical significance level of 5%).

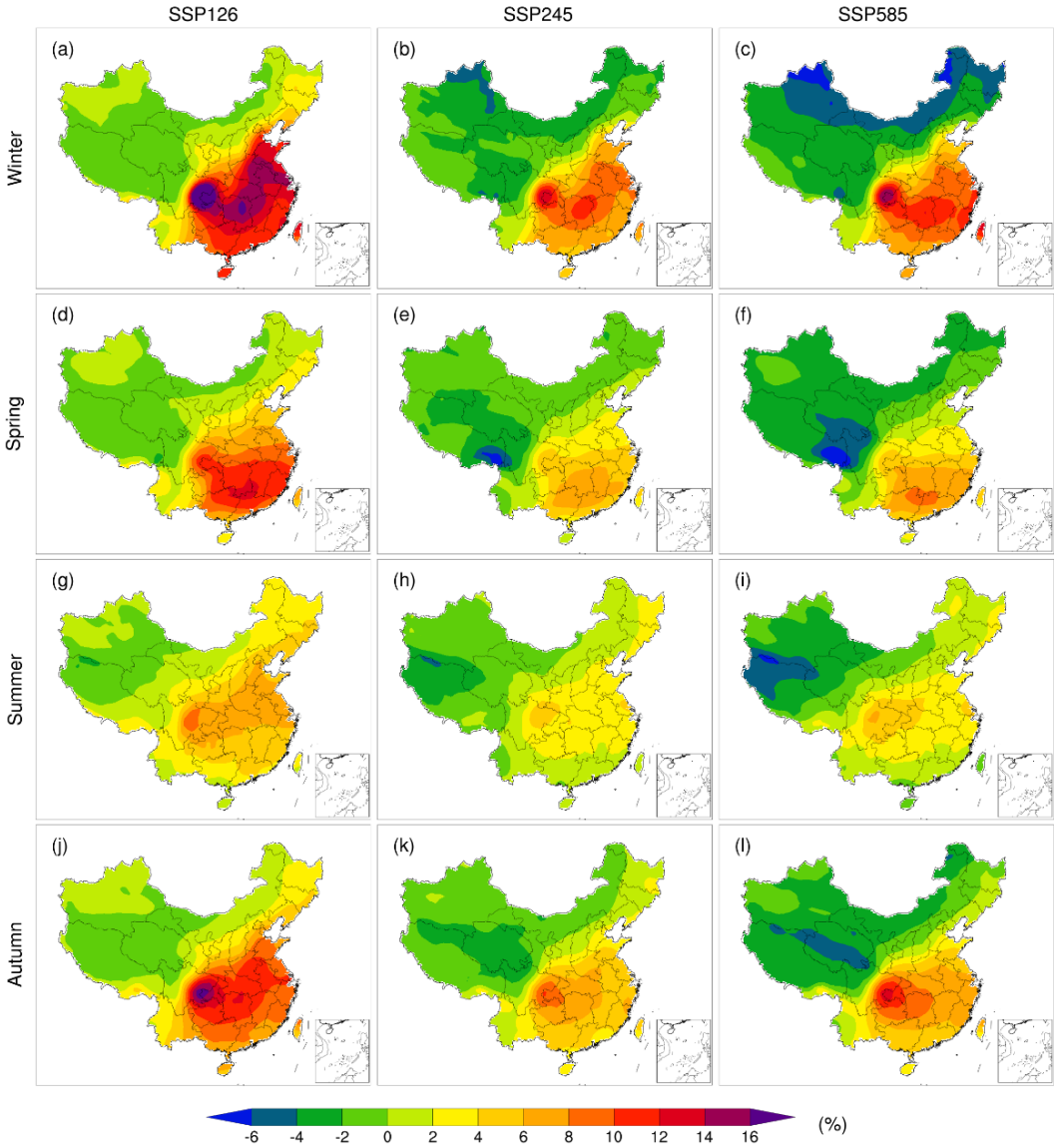

Figure 8. Percentage changes in seasonal photovoltaic generation under the SSP126 (first column), SSP245 (second column) and SSP585 (third column) scenarios. Maps show differences between 2051-2070 and 1995-2014 in the multi-model mean, calculated as future minus reference. The rows depict the changes in winter, spring, summer and autumn.

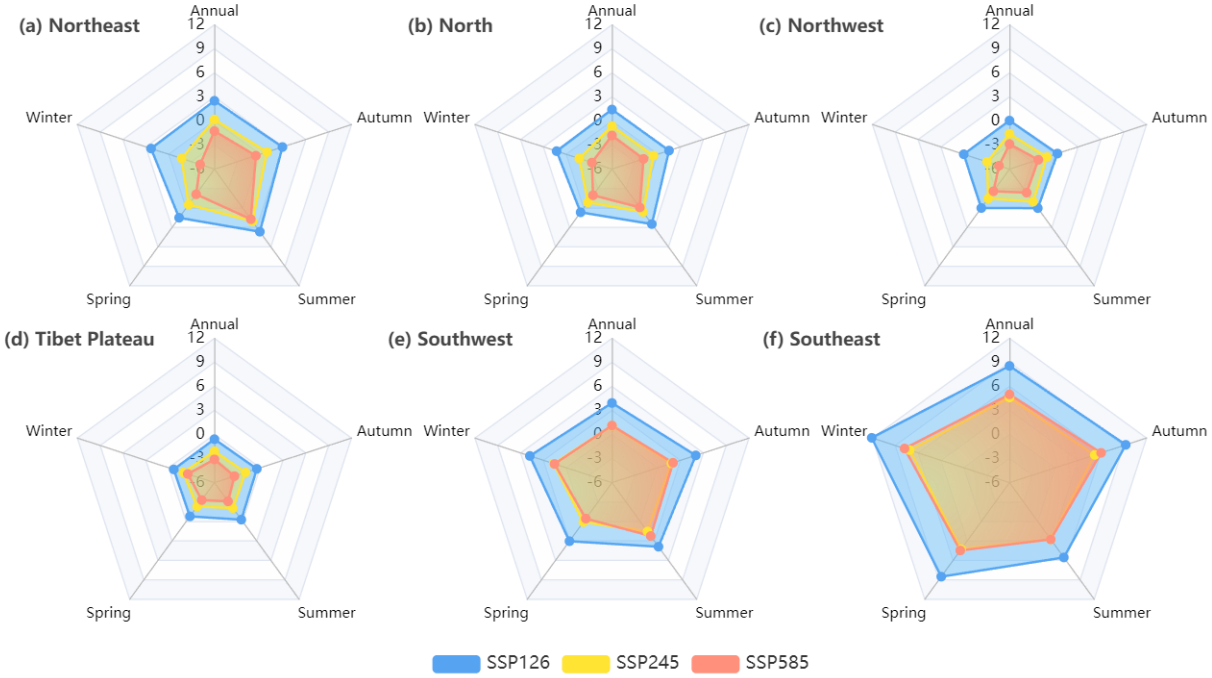

Figure 9. The spider map of changes in seasonal PV generation over the subregions of China under SSP126, SSP245 and SSP585 scenarios (Unit: %). The five axes of spider map represent the changes in annual, winter, spring, summer and autumn.

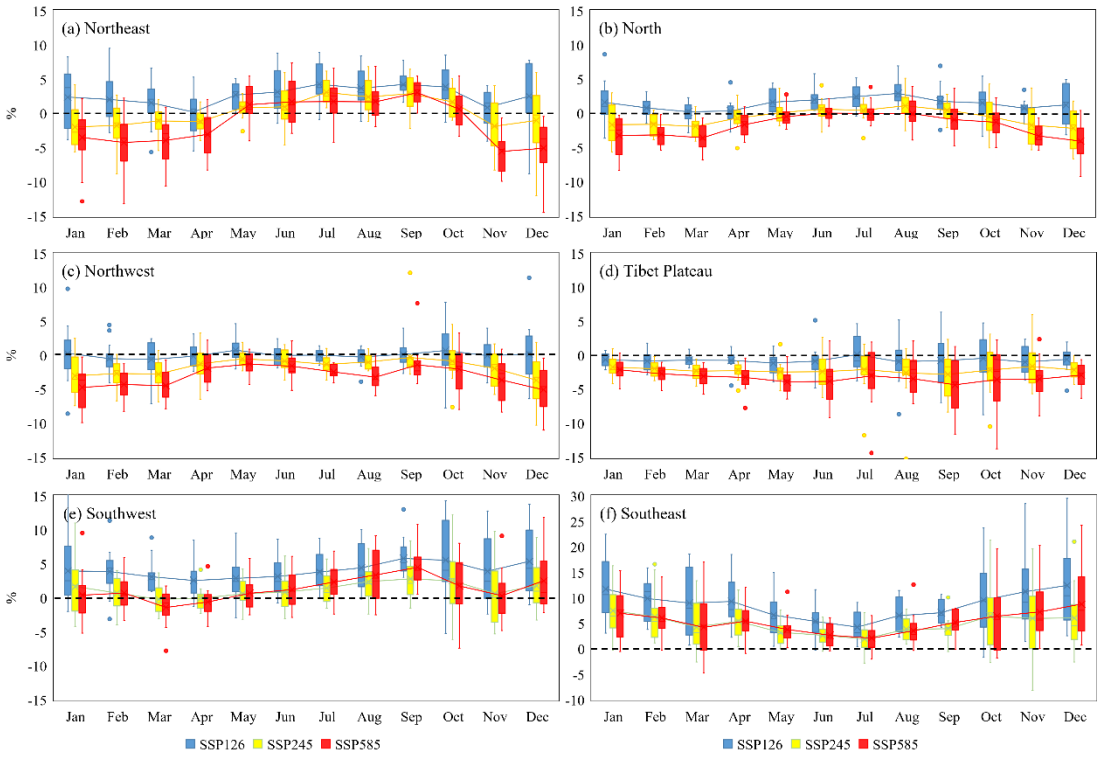

Figure 10. Box-whisker plots of PV power generation changes (%) for CMIP6 models in six subregions over China under SSP126, SSP245 and SSP585 scenarios. The whiskers indicate the minimum and maximum changes, and the boxes represent the 25th to 75th percentile. The black dotted line represents the baseline of the historical period and the solid lines are the mean line of different scenarios.

References

[1] Intergovernmental Panel on Climate Change. Summary for Policymakers" in Global warming of 1.5° C. An IPCC Special Report on the impacts of global warming of 1.5° C above pre-industrial levels and related global greenhouse gas emission pathways, in the context of strengthening the global response to the threat of climate change, sustainable development, and efforts to eradicate poverty. World Meteorological Organization Geneva, Switzerland; 2018. p. 32.

[2] Huang M-T, Zhai P-M. Achieving Paris Agreement temperature goals requires carbon neutrality by middle century with far-reaching transitions in the whole society. Adv Clim Change Res. 2021;12:281-6.

[3] Zhou S, Tong Q, Pan X, Cao M, Wang H, Gao J, et al. Research on low-carbon energy transformation of China necessary to achieve the Paris agreement goals: A global perspective. Energy Econ. 2021;95:105137.

[4] You M, Liu P. The Carbon Puzzle: Examining the Impact of China's "30• 60 Dual-Carbon Target" on Carbon-Intensive and Green Firms. Available at SSRN 4016959. 2022.

[5] Carvalho D, Rocha A, Gómez-Gesteira M, Santos CS. Potential impacts of climate change on European wind energy resource under the CMIP5 future climate projections. Renewable Energy. 2017;101:29-40.

[6] Zhuo C, Junhong G, Wei L, Fei Z, Chan X, Zhangrong P. Changes in wind energy potential over China using a regional climate model ensemble. Renewable Sustainable Energy Rev. 2022;159.

[7] International Energy Agency. Solar PV. 2022.

[8] Renewable Energy Policy Network for the 21st Century. Renewables 2022 Global Status Report. 2022.

[9] Qiu T, Wang L, Lu Y, Zhang M, Qin W, Wang S, et al. Potential assessment of photovoltaic power generation in China. Renewable Sustainable Energy Rev. 2022;154:111900.

[10] Anandh T, Gopalakrishnan D, Mukhopadhyay P. Analysis of future wind and solar potential over India using climate models. Curr Sci. 2022;122:1268.

[11] Wild M, Folini D, Henschel F, Fischer N, Müller B. Projections of long-term changes in solar radiation based on CMIP5 climate models and their influence on energy yields of photovoltaic systems. Sol Energy. 2015;116:12-24.

[12] Dutta R, Chanda K, Maity R. Future of solar energy potential in a changing climate across the world: A CMIP6 multi-model ensemble analysis. Renewable Energy. 2022;188:819-29.

[13] Hasni A, Sehli A, Draoui B, Bassou A, Amieur B. Estimating global solar radiation using artificial neural network and climate data in the south-western region of Algeria. Energy Procedia. 2012;18:531-7.

[14] Guermoui M, Gairaa K, Rabehi A, Djafer D, Benkaciali S. Estimation of the daily global solar radiation based on the Gaussian process regression methodology in the Saharan climate. The European Physical Journal Plus. 2018;133:1-17.

[15] Doorga JR, Rughooputh SD, Boojhawon R. Modelling the global solar radiation climate of Mauritius using regression techniques. Renewable Energy. 2019;131:861-

78.
[16] Behar O, Khellaf A, Mohammedi K. Comparison of solar radiation models and their validation under Algerian climate–The case of direct irradiance. Energy Convers Manage. 2015;98:236-51.
[17] Samadianfard S, Majnooni-Heris A, Qasem SN, Kisi O, Shamshirband S, Chau K-w. Daily global solar radiation modeling using data-driven techniques and empirical equations in a semi-arid climate. Eng Appl Comput Fluid Mech. 2019;13:142-57.
[18] Holmgren WF, Hansen CW, Mikofski MA. pvlib python: A python package for modeling solar energy systems. Journal of Open Source Software. 2018;3:884.
[19] Jiang H, Yao L, Lu N, Qin J, Liu T, Liu Y, et al. Geospatial assessment of rooftop solar photovoltaic potential using multi-source remote sensing data. Energy AI. 2022;10:100185.
[20] Yadav AK, Chandel S. Solar radiation prediction using Artificial Neural Network techniques: A review. Renewable Sustainable Energy Rev. 2014;33:772-81.
[21] Behrang M, Assareh E, Ghanbarzadeh A, Noghrehabadi A. The potential of different artificial neural network (ANN) techniques in daily global solar radiation modeling based on meteorological data. Sol Energy. 2010;84:1468-80.
[22] Shboul B, Ismail A-A, Michailos S, Ingham D, Ma L, Hughes KJ, et al. A new ANN model for hourly solar radiation and wind speed prediction: A case study over the north & south of the Arabian Peninsula. Sustainable Energy Technol Assess. 2021;46:101248.
[23] Wu J, Shi Y, Xu Y. Evaluation and projection of surface wind speed over China based on CMIP6 GCMs. J Geophys Res: Atmos. 2020;125:e2020JD033611.
[24] Zou L, Wang L, Li J, Lu Y, Gong W, Niu Y. Global surface solar radiation and photovoltaic power from Coupled Model Intercomparison Project Phase 5 climate models. J Cleaner Prod. 2019;224:304-24.
[25] Ji L, Wu Y, Sun L, Zhao X, Wang X, Xie Y, et al. Solar photovoltaics can help China fulfill a net-zero electricity system by 2050 even facing climate change risks. Resour Conserv Recycl. 2022;186:106596.
[26] Zhao X, Huang G, Lu C, Zhou X, Li Y. Impacts of climate change on photovoltaic energy potential: A case study of China. Appl Energy. 2020;280:115888.
[27] Zhang S, Li X. Future projections of offshore wind energy resources in China using CMIP6 simulations and a deep learning-based downscaling method. Energy. 2021;217:119321.
[28] Wu J, GAO X-J. A gridded daily observation dataset over China region and comparison with the other datasets. Chin J Geophys. 2013;56:1102-11.
[29] Pfenninger S, Staffell I. Long-term patterns of European PV output using 30 years of validated hourly reanalysis and satellite data. Energy. 2016;114:1251-65.
[30] Ridley B, Boland J, Lauret P. Modelling of diffuse solar fraction with multiple predictors. Renewable Energy. 2010;35:478-83.
[31] Müller J, Folini D, Wild M, Pfenninger S. CMIP-5 models project photovoltaics are a no-regrets investment in Europe irrespective of climate change. Energy. 2019;171:135-48.
[32] Huld T, Gottschalg R, Beyer HG, Topič M. Mapping the performance of PV

modules, effects of module type and data averaging. Sol Energy. 2010;84:324-38.
[33] Taylor KE. Summarizing multiple aspects of model performance in a single diagram. J Geophys Res: Atmos. 2001;106:7183-92.
[34] Zhu H, Jiang Z, Li L. Projection of climate extremes in China, an incremental exercise from CMIP5 to CMIP6. Sci Bull. 2021;66:2528-37.
[35] Jiang Z, Li W, Xu J, Li L. Extreme precipitation indices over China in CMIP5 models. Part I: Model evaluation. J Clim. 2015;28:8603-19.
[36] Li W, Jiang Z, Xu J, Li L. Extreme precipitation indices over China in CMIP5 models. Part II: probabilistic projection. J Clim. 2016;29:8989-9004.
[37] Administration NE. Construction and operation of photovoltaic power generation in 2021. 2022.
[38] Elhadidy MA. Performance evaluation of hybrid (wind/solar/diesel) power systems. Renewable Energy. 2002;26:401-13.
[39] Qiu L, He L, Lu H, Liang D. Systematic potential analysis on renewable energy centralized co-development at high altitude: A case study in Qinghai-Tibet plateau. Energy Convers Manage. 2022;267:115879.
[40] Duan P. Research on the transaction and settlement mechanism of Yunnan clean energy's participation in the west to East power transmission for the goal of "carbon peak" and "carbon neutral". 2021 IEEE Sustainable Power and Energy Conference (iSPEC): IEEE; 2021. p. 1843-50.
[41] Abolude AT, Zhou W, Akinsanola AA. Evaluation and projections of wind power resources over China for the energy industry using CMIP5 models. Energies. 2020;13:2417.
[42] Guo J, Huang G, Wang X, Li Y. Improved performance of a PRECIS ensemble in simulating near- surface air temperature over China. Clim Dyn. 2019;52:6691-704.
[43] Bryce R, Carreño IL, Kumler A, Hodge B-M, Roberts B, Martinez-Anido CB. Consequences of neglecting the interannual variability of the solar resource: A case study of photovoltaic power among the Hawaiian Islands. Sol Energy. 2018;167:61-75.
[44] Li X, Wagner F, Peng W, Yang J, Mauzerall DL. Reduction of solar photovoltaic resources due to air pollution in China. Proceedings of the National Academy of Sciences. 2017;114:11867-72.
[45] Sweerts B, Pfenninger S, Yang S, Folini D, Van der Zwaan B, Wild M. Estimation of losses in solar energy production from air pollution in China since 1960 using surface radiation data. Nat Energy. 2019;4:657-63.
[46] Ohunakin OS, Adaramola MS, Oyewola OM, Matthew OJ, Fagbenle RO. The effect of climate change on solar radiation in Nigeria. Sol Energy. 2015;116:272-86.
[47] Kjellstro¨ M E, Nikulin G, Hansson U, Strandberg G, Ullerstig A. 21st century changes in the European climate: uncertainties derived from an ensemble of regional climate model simulations. Tellus A: Dyn Meteorol Oceanogr. 2011;63:24-40.
[48] Palmer T, Shutts G, Hagedorn R, Doblas-Reyes F, Jung T, Leutbecher M. Representing model uncertainty in weather and climate prediction. Annu Rev Earth Planet Sci. 2005;33:163-93.